arXiv:2102.03571v2 [physics.flu-dyn] 14 Oct 2021

Two-dimensionally stable self-organization arises in simple schooling swimmers through hydrodynamic interactions

Melike Kurt[a], **Pedro Costa Ormonde**[b], **Amin Mivehchi**[b], **and Keith W. Moored**[b,1]

[a]Aerodynamics and Flight Mechanics Group, Faculty of Engineering and the Environment, University of Southampton, Southampton SO17 1BJ, UK; [b]Mechanical Engineering and Mechanics, Lehigh University, Bethlehem, PA, 18015, USA

We present new constrained and free-swimming experiments and simulations of a pair of pitching hydrofoils interacting in a minima school. The hydrofoils have an out-of-phase synchronization and they are varied through in-line, staggered, and side-by-side arrangements within the two-dimensional interaction plane. It is discovered that there is a *two-dimensionally* stable equilibrium point for a side-by-side arrangement. In fact, this arrangement is super-stable, meaning that hydrodynamic forces will passively maintain this arrangement even under external perturbations and the school as a whole has no net forces acting on it, causing it to drift to one side or the other. Moreover, previously discovered *one-dimensionally* stable equilibria driven by wake vortex interactions are shown to be, in fact, two-dimensionally *unstable*, at least for an out-of-phase synchronization. Additionally, it is discovered that a trailing-edge vortex mechanism provides the restorative force to stabilize a side-by-side arrangement and the stable equilibrium is further verified for freely-swimming foils where dynamic recoil motions are present. When constrained, the swimmers experience a collective thrust and efficiency increase up to 100% and 40%, respectively, in a side-by-side arrangement, whereas the staggered arrangements output an even higher efficiency improvement of 87% with a 94% increase in thrust. For freely-swimming foils, the recoil motion attenuates the improvements at the stable equilibrium, showing a more modest speed and efficiency enhancement of up to 9% and 6%, respectively. These newfound schooling performance and stability characteristics suggest that fluid-mediated equilibria may play a role in the control strategies of schooling fish and fish-inspired robots.

collective locomotion | hydrodynamic interactions | fish schooling | pattern formation | collective performance

Self-organization of living systems is one of Nature's most ubiquitous and mesmerizing phenomena. It arises across a wide range of spatial and temporal scales from the cells in our bodies (1) and swarming of microorganisms (2) to the flocking of birds (3) and schooling of fish (4). For macroscopic flyers and swimmers, a wide range of hypotheses have attributed collective behavior to social interactions (5), protection against predators (6), food prospect optimization (7), and/or energetic benefits (4). Our knowledge of the latter hypothesis is limited since it is regulated by complex hydrodynamic interactions. Yet, both the spatial organization (3, 8) and temporal synchronization (9–11) have emerged as factors influencing the hydrodynamic interactions, and, consequently, the energetic cost of locomotion and traveling speed of individuals in a collective. Still, our understanding of the force production and energetics of schooling swimmers is mostly limited to canonical spatial arrangements such as a leader-follower in-line arrangement (12–15) and a side-by-side arrangement (11, 16–18), while there are fewer studies of staggered arrangements (19–22).

Because of these studies it is commonly presumed that the spatial organization observed in schools is driven by the interest to maximize swimming efficiency or force production. However, another explanation was first proposed by Sir James Lighthill (23). The so-called Lighthill conjecture (24) postulates that the arrangements of fish in a school may be due to the interaction forces that push and pull the swimmers into a particular stable formation, much like the atoms in a crystal lattice. Indeed, this idea of passive self-organization has shown promise in recent studies where one-dimensional streamwise stability has been observed in pairs of in-line self-propelled foils (24, 25) or in small schools of various arrangements (20, 26), as well as in pairs of in-line hydrofoils with differing kinematics (27). While these studies have shown seminal results supporting the Lighthill conjecture, they have only probed the one-dimensional stability of arrangements. However, *two-dimensionally* or even three-dimensionally stable arrangements are required for the passive self-organization of schools that produce two-dimensional or three-dimensional flows.

Here, we advance our understanding of the hydrodynamic interactions of schooling swimmers in two ways. For the first time, we measure the *two-dimensional* stability of schooling

Significance Statement

Fish schools are fascinating examples of self-organization in nature. They serve many purposes from enhanced foraging, and protection to improved socialization and migration. However, our understanding of the hydrodynamic interactions in schools is primitive. It has been postulated that these interactions can regulate energy usage and speed, as well as push and pull individuals thereby altering the school's structure and function. We have discovered that stable arrangements of swimmers can arise in two-dimensional schools through passive hydrodynamic forces alone. In these stable arrangements, swimmers also experience speed and efficiency benefits. This opens the door to considering that the structure and function of fish schools may be more strongly regulated by hydrodynamic interactions than previously known.

M. K. helped design the study, gathered and processed constrained-foil measurements, and drafted the manuscript. P. C. O. helped design the study, gathered and processed the unconstrained-foil data, and helped revise the manuscript. A. M. helped design the study, gathered and processed the numerical and the flow-visualization data, and helped revise the manuscript. K. W. M. helped design the study, and helped revise the manuscript.

The authors declare no conflict of interest.

[1]To whom correspondence should be addressed. E-mail: kmoored@lehigh.edu

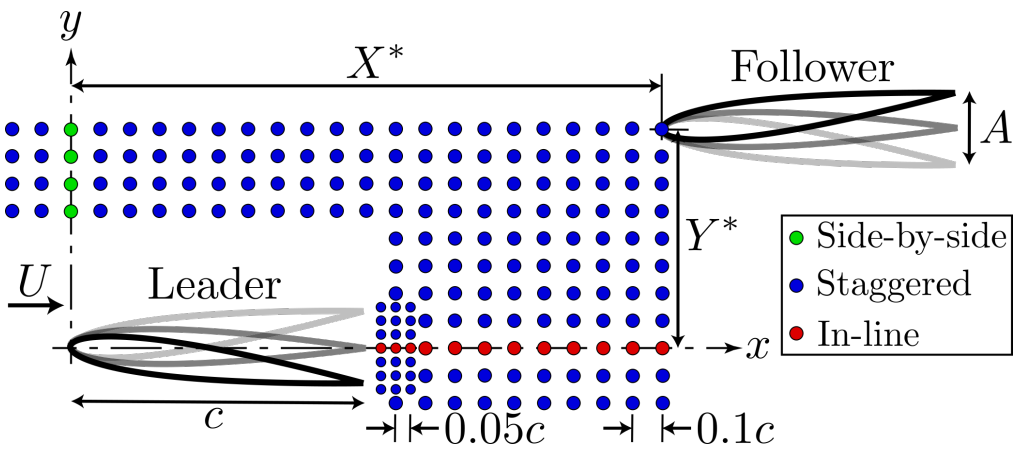

Fig. 1. Schematic of positions of the follower hydrofoil relative to the leader. Shown are two coarse rectangular grids of 0.1c spacing ranging from $-0.2 \leq X^* \leq 2$, $0.5 \leq Y^* \leq 0.8$, and $1.1 \leq X^* \leq 2$, $-0.2 \leq Y^* \leq 0.4$, as well as a refined rectangular grid of 0.05c spacing ranging from $1.05 \leq X^* \leq 1.15$, $-0.15 \leq Y^* \leq 0.15$. In total there are 180 grid points.

arrangements for constrained and unconstrained foils, which takes us closer to understanding the role of the Lighthill conjecture in schooling formations. We discover that many of the one-dimensionally stable formations previously observed are, in fact, unstable once the cross-stream stability is considered. Yet, we still find that a side-by-side arrangement is *two-dimensionally* stable providing support for the hypothesis that this arrangement observed in real fish (11) may be due to passive self-organization. Second, we measure the force production and energetics of two interacting hydrofoils throughout a plane of possible arrangements ranging from in-line to side-by-side by passing through the possible staggered arrangements. We reveal that there is a thrust and efficiency optimum in a slightly-staggered arrangement where there is direct vortex impingement on the follower.

Experimental Approach and Results

To examine the flow interactions that occur in schools, full swimmer models can be readily used in numerical studies (19), however, these models are difficult to implement experimentally. Instead, experiments typically use oscillating hydrofoils as a simple model of the propulsive appendages of animals (12–14, 16, 17, 22, 24, 25, 27, 28). Importantly, these oscillating hydrofoils capture the salient unsteady fluid mechanics of the added mass forces, circulatory forces, and shed vortices.

Following this simple model approach, experiments were conducted on a pair of pitching hydrofoils immersed in a water channel, forming a minimal school or minimal collective. The flow over the hydrofoils was restricted to be nominally two-dimensional. The arrangement of the hydrofoils was varied by manipulating the follower hydrofoil position in the streamwise and cross-stream directions as shown in Figure 1. The dimensionless distances were normalized by the chord length as $X^* = x/c$, and $Y^* = y/c$. The leader hydrofoil was prescribed a sinusoidal pitching motion of $\theta_L(t) = \theta_0 \sin(2\pi ft)$, where the oscillation frequency is f, and the pitching amplitude is θ_0, which is related to the peak-to-peak trailing edge amplitude as $A = 2c\sin(\theta_0)$. The follower was pitched similarly as $\theta_F(t) = \theta_0 \sin(2\pi ft + \phi)$ with a fixed phase difference or synchrony of $\phi = \pi$ throughout the study. Moreover, the oscillation frequency and the dimensionless amplitude, $A^* = A/c$, were also fixed throughout the study at $f = 0.98$ Hz and $A^* = 0.25$, which gives a fixed reduced frequency of $k = fc/U = 1$, and a fixed Strouhal number of $St = fA/U = 0.25$. These dimensionless numbers are typical of efficient biological swimming (29, 30). Direct force measurements were taken from each hydrofoil at every (X^*, Y^*) position, which corresponds to a total of 180 arrangements in the x-y plane. For further information about the water channel setup, actuator mechanisms, sensors, the methods used, and the definition of the performance coefficients for an individual hydrofoil as well as the collective, please see *Materials and Methods* and *Supplementary Information*.

Follower Force Map. In order to probe the Lighthill conjecture in two-dimensions, the *relative forces* acting on the follower in the (x-y) interaction plane must be examined. This is done by constructing a *force map*, which is described below.

Consider a frame of reference attached to the leader as in Figure 1. The relative lift, ΔL, in the cross-stream direction and the relative thrust, ΔT, in the streamwise direction are defined simply as a difference between the forces acting on the two hydrofoils as $\Delta T = T_F - T_L$ and $\Delta L = L_F - L_L$, where forces acting on the leader and follower hydrofoils are denoted with $(.)_L$ and $(.)_F$, respectively. Figure 2A and 2B show the relative force conditions that leads to the follower either moving towards or moving away from the leader in the streamwise (x) and cross-stream (y) directions.

First, consider the relative lift for the positive x-y plane. The follower is pushed away from the leader in the cross-stream direction ($\updownarrow$) when the relative lift force is greater than zero (Figure 2A). This condition arises either when lift forces acting on the foils are in the same direction and $L_F > L_L$, or when they are acting in opposite directions and pointing away from each other ($L_L < 0 \downarrow$, $L_F > 0 \uparrow$). In contrast, the follower is pulled towards the leader when the lift forces are acting in the same direction and $L_L > L_F$ or acting in opposite directions and pointing towards each other ($L_L > 0 \uparrow$, $L_F < 0 \downarrow$).

Next, consider the relative thrust force in the positive x-y plane. A positive relative thrust force ($\Delta T > 0$) acts to move the follower towards the leader, which arises when $T_F > T_L$. In contrast, when $T_L > T_F$ the relative thrust force is negative ($\Delta T < 0$) and the follower moves away from the leader in the

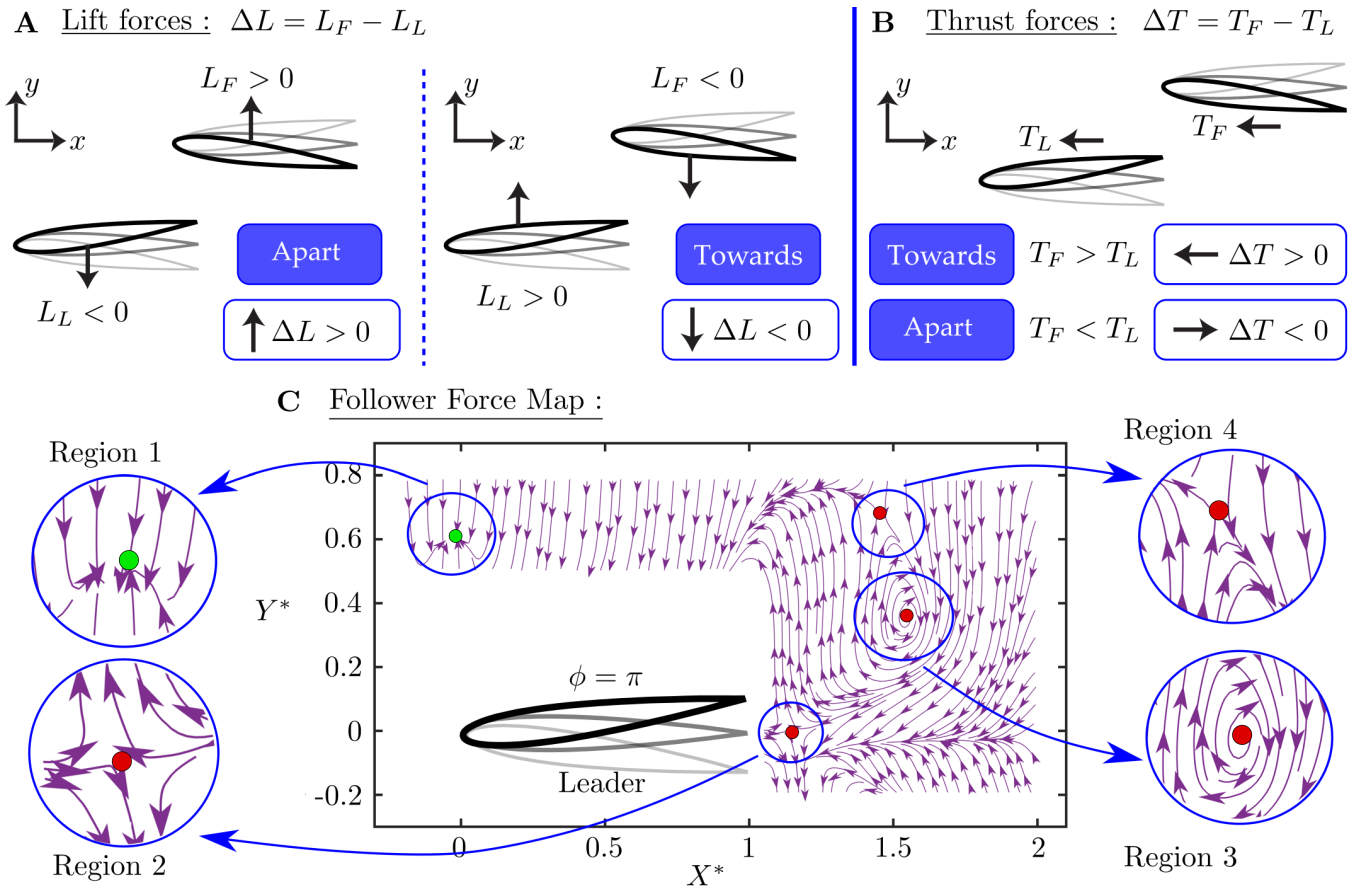

Fig. 2. Typical conditions leading to positive and negative relative (A) lift and (B) thrust. (C) Follower force map with an out-of-phase synchrony between the leader and follower, i.e. $\phi = \pi$. The arrows on the force lines indicate the direction that the follower would move in relative to the leader if it were free-swimming. The green and red circles represent the stable and unstable equilibria, respectively.

streamwise direction as shown in Figure 2B. If $T_L = T_F$ then the leader and follower swim at the same speed and do not move closer or apart.

To visualize the directions of the relative forces acting on the follower throughout the x-y plane we constructed a force map, which is a novel visualization made up of force lines (Figure 2C). Put simply, the force map conveys *the direction that the follower would move in as observed by the leader.* The force map is constructed with the origin located at the leading edge of the leader and a relative force vector ($\mathbf{F}_{\text{rel}} = -\Delta T\hat{\mathbf{x}} + \Delta L\hat{\mathbf{y}}$) is determined at each of the measurement positions detailed in Figure 1, such that a relative force vector field is created. Force lines are then graphed as lines that are everywhere tangent to the local relative force vector field, analogous to streamlines.

Observed Equilibria. The force map reveals four critical points or equilibria where the relative force vector is equal to zero, that is, $\Delta T = 0$ and $\Delta L = 0$, which are marked by green and red circles in Figure 2C. The first equilibrium point is located at $(X^*, Y^*) = (0, 0.6)$ in Region 1 where the leader and follower are interacting in a *side-by-side* arrangement. Interestingly, as the force lines merge at this point, their direction indicates that this critical point is a *stable equilibrium point* in two-dimensions. Therefore, when any perturbations move the follower away from this point, forces will arise to return the foil back to this location. Previous low Reynolds number simulations have also shown that side-by-side arrangements of bending foils are two-dimensionally stable (20), at least for foils constrained in the cross-stream direction. Another critical point in Region 2 is located at $(X^*, Y^*) = (1.2, 0)$ in the leader's wake where the follower is directly *in-line* with the leader. Region 2 represents an equilibrium point that is stable to streamwise perturbations, but unstable to cross-stream perturbations, that is, an *unstable saddle point.* In Region 3 there is an equilibrium point located at $(X^*, Y^*) = (1.6, 0.3)$ representing a *staggered* arrangement of the foils. This equilibrium point represents an *unstable source point* where the force-lines spiral outward from it. Finally, Region 4 reveals another *unstable saddle point* for a staggered arrangement with the follower located at $(X^*, Y^*) = (1.5, 0.7)$.

By definition the mean forces go to zero at the equilibria, however, the thrust and lift forces exhibit fluctuations as the foils undergo pitching motions. In order to understand this aspect, we analyzed the lift and thrust fluctuations of the leader and follower as presented in Figure S3 in the *Supplementary Information.* Overall, the lift fluctuations are found to be an order of magnitude higher than the thrust fluctuations for the constrained foils, as previously observed in (31) for a pair of interacting fish through 3D computations. At the

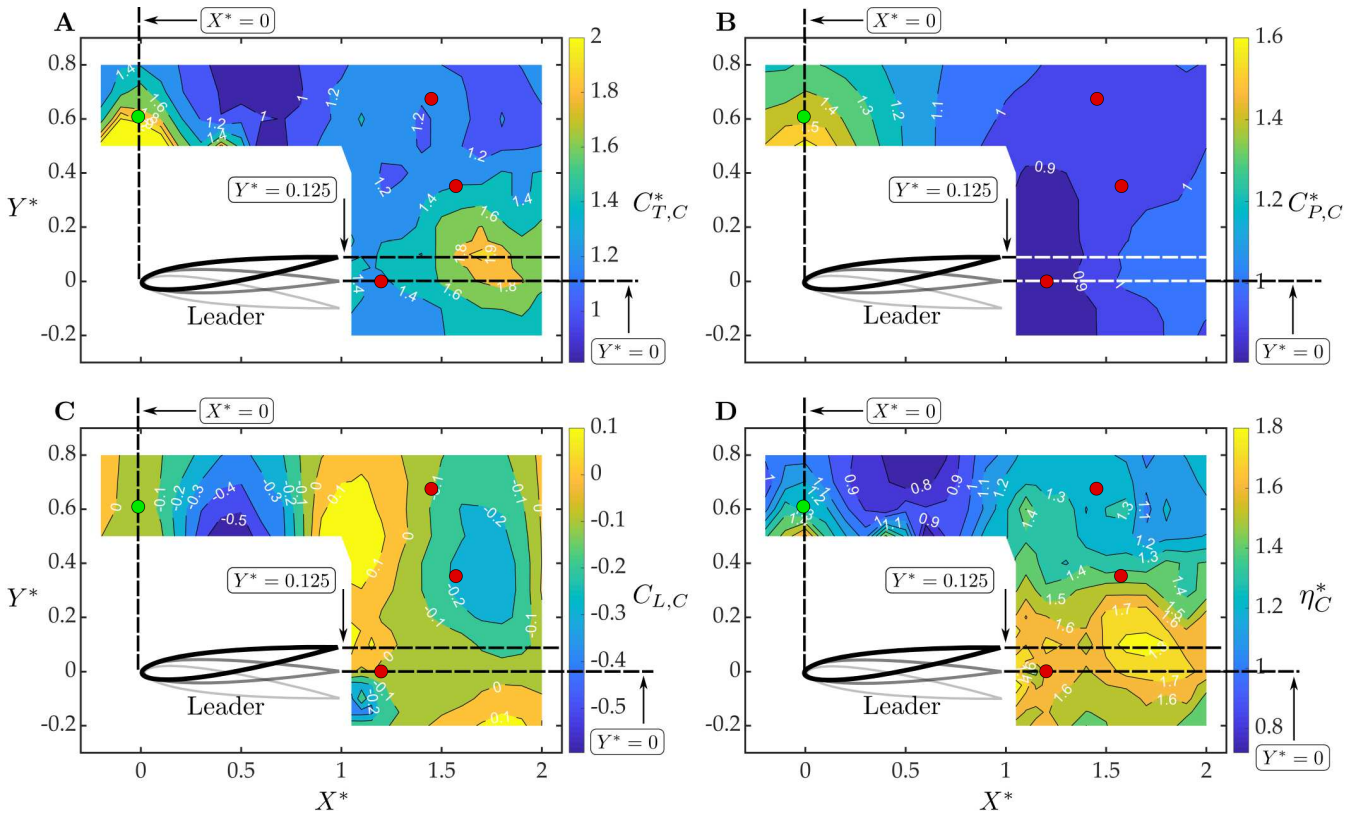

Fig. 3. Contour maps of normalized collective (A) thrust, and (B) power, (C) collective lift, and (D) normalized collective efficiency. The black dashed lines show the locations corresponding to $X^* = 0$, $Y^* = 0$, and $Y^* = 0.125$. The leader position, size, and amplitude of motion is shown for reference. The green and red circles represent the stable and unstable equilibria, respectively, from Figure 2.

stable side-by-side equilibrium, the lift and thrust fluctuations increase by 30-40% over an isolated hydrofoil. When unconstrained (freely swimming), this may cause the foils to undergo larger amplitude recoil motions and the arrangement to no longer be stable. Around the in-line unstable equilibrium, the force fluctuations on both foils are, surprisingly, reduced compared to an isolated hydrofoil. At the other equilibria, the fluctuations stay effectively at about the same levels as an isolated hydrofoil. Also, in the wake of the leader around $1.5 \leq X^* \leq 2$, there is an increase in the follower's lift and thrust fluctuations by 20-40%.

Collective Performance. Beyond probing the Lighthill conjecture in two dimensions, the collective performance was also measured in the same interaction plane. Figure 3 presents the normalized collective thrust, $C^*_{T,C}$, and power, $C^*_{P,C}$, the collective lift, $C_{L,C}$, and the normalized collective efficiency, η^*_C, as a contour map of (X^*, Y^*). The normalized performance metrics compare the collective performance of the leader-follower pair with that of two *isolated* hydrofoils. Note that in contrast to the relative forces that were discussed in the previous section, a *collective* lift of zero does not necessarily mean zero lift for the foils individually.

Figure 3A shows the normalized collective thrust as a function of the streamwise and cross-stream position of the follower relative to the leader. Generally, the collective thrust stays within the range of $1 \leq C^*_{T,C} \leq 2$, which indicates that the collective performs better than two hydrofoils in isolation for nearly the entire interaction plane considered here. Previous work has also observed similar thrust enhancements albeit for a limited set of data of one side-by-side and two staggered arrangements at $Y^* = 1$ (32). The peaks in collective thrust can be grouped into two regions. First, is a region enclosing the side-by-side arrangements, along the line of $X^* = 0$ (black dashed line), where the collective is found to achieve $40-100\%$ higher thrust than in isolation. Recent work has established (33) that the thrust increase for out-of-phase pitching foils in this region originates from an increase in their added mass. It was determined that the added mass thrust dominates the thrust production of pitching foils and thereby wake effects play no significant role in their thrust increase. However, for heaving or combined heaving and pitching foils, wake effects, and circulatory forces in general, are expected to be important for thrust production in a side-by-side arrangement (34). A second region corresponds to the direct wake interactions enclosing the in-line and staggered arrangements, within the region of $0 \leq Y^* \leq 0.3$. For the in-line arrangements, the collective thrust reaches a 74% peak increase over the hydrofoils in isolation, whereas, the thrust reaches a 94% peak increase for slightly-staggered arrangements along the $Y^* = 0.125$ line. This line is where direct wake vortex impingement onto the follower is anticipated. It has already been established that wake-body impingement interactions generate increased thrust through an increase in the effective angle of attack of the follower and are therefore circulatory in nature (12, 13).

Figure 3B presents the normalized collective power in the interaction plane. For near wake interactions where the collective is in in-line or staggered arrangements ($X^* > 1.1$ and

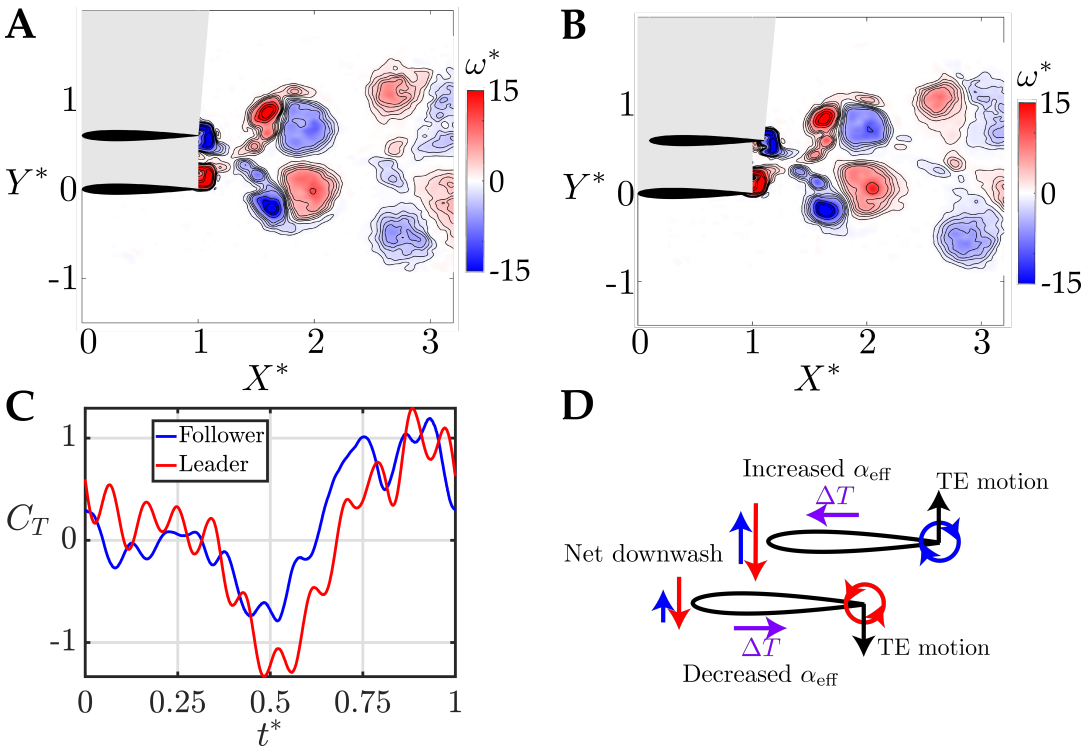

Fig. 4. (A) Vorticity field for the stable side-by-side arrangement ($X^* = 0$, $Y^* = 0.6$) at $t^* = 0.5$ when the foils are pitching away from each other. (B) Vorticity field for the arrangement of $X^* = 0.1$, $Y^* = 0.6$ at $t^* = 0.5$. (C) The time-varying thrust coefficient of the leader and follower at $X^* = 0.4$, $Y^* = 0.6$. (D) Schematic of proposed trailing-edge vortex mechanism responsible for a restorative force back to the stable side-by-side arrangement.

any Y^*), the collective power exhibits little variation from the isolated case, whereas, the side-by-side arrangements result in up to a 50% increase in power.

Similarly, the collective lift coefficient is presented in Figure 3C. For side-by-side arrangements, where a stable equilibrium point is located, the collective lift generation is found to be negligible. This means that when two individuals are swimming in this stable arrangement, the arrangement is, in fact, *super-stable*, that is, the relative distances between the swimmers do not change *and* the pair of swimmers will remain swimming forward without a collective drift to one side or another. Likewise, for the in-line interaction region, where an unstable equilibrium point is located, collective lift generation is found to be negligible as well.

In Figure 3D, the collective efficiency is observed to increase by $10-40\%$ over that of isolated foils for the side-by-side interaction region, which has been observed previously (32). In the in-line interaction region, even higher peak efficiency increases are identified with up to a 74% increase for in-line interactions and an 87% increase for slightly-staggered arrangements along the $Y^* = 0.125$ dashed line. It is clear that while both the side-by-side and in-line interaction regions see comparable thrust increases, the efficiency increase in the side-by-side interaction is tempered by a concurrent rise in power, whereas the efficiency increase in the in-line interaction region is solely driven by the increase in thrust. Some previous work has not observed an efficiency benefit for staggered arrangements with $Y^* = 1$ (32), however, in the near-wake interactions probed in the current study with $Y^* \leq 0.8$ it is revealed that the greatest efficiency benefits are observed for slightly staggered arrangements.

Wake Dynamics and Time-Varying Forces. To understand the flow mechanisms behind the stable side-by-side arrangement and the high-efficiency slightly-staggered arrangement particle image velocimetry (PIV) measurements are paired with the leader and follower's time-varying forces.

Figure 4A presents the vorticity shed from the leader and follower at the stable side-by-side equilibrium at a dimensionless time of $t^* = t/T = 0.5$ where the foils are pitching away from each other. The forming clockwise vortex of the follower and counterclockwise vortex of the leader mutually induce each other in a way that slows their downstream advection. These vortices then pair with their counter-rotating counterparts shed a half cycle later. The pairs mutually induce away from the symmetry line between the foils, leading to momentum jets behind the foils that deflect away from the symmetry line. The deflected jet and vortex pairing mechanism were first observed in (17) and later in subsequent work (35).

The cross-stream stability of the side-by-side arrangement is mediated by a balance of the wake-induced forces from the deflected jet and the quasi-steady forces, that is, the body-body flow interaction between the foils, which has been established in (28). Furthermore, studies examining the interaction of two side-by-side *undulatory* swimmers have also observed deflected wake interactions albeit with a less pronounced deflection (36). In fact, for some cases of undulatory swimmers very little if any jet deflection is noticeable (37, 38) indicating that the lift forces mediating the stable equilibria may be quite weak in some cases as observed in (37).

It has already been established in (33) that the thrust increase with decreasing separation distance between the side-by-side leader and follower foils originates from an increase in

the added mass thrust of the two foils, which dominates the thrust production of pitching foils (39, 40). The increase in added mass and influence of the shedding vortices from the interacting foils also increase the power, though, not quite as much as the thrust giving rise to a small increase in efficiency as the foils get closer to each other (33).

What is not established yet is the mechanism that generates restorative thrust forces for the leader and follower to bring them back to the side-by-side equilibrium when one of them is perturbed downstream of the other. Figure 4B shows the vorticity field at a dimensionless time of $t^* = 0.5$ when the follower is located slightly downstream of the side-by-side equilibrium arrangement at $(X^*, Y^*) = (0.1, 0.6)$. The wakes of the leader and follower show the same vortex pairs as observed at the equilibrium arrangement with a slight asymmetry. Figure 4C presents the time-varying thrust of the leader and follower for an arrangement that is perturbed further downstream at $X^* = 0.4$ and $Y^* = 0.6$ where the difference in the leader and follower thrust is more pronounced. When the follower is perturbed downstream it produces more thrust than the leader around $t^* = 0.5$, which acts to increase the swimming speed of the follower and restore the two foils back to the stable equilibrium. Figure 4D shows a schematic that describes the flow mechanism behind these restorative forces. When the follower is perturbed downstream, the forming counterclockwise vortex of the leader is closer to the leading edge of the follower (as observed in 4B), which leads to an increase in the downwash acting on the follower. Since the foils are pitching away from each other, this downwash increases the effective angle of attack of the follower, thereby increasing its thrust production. In the same arrangement, the forming clockwise vortex from the follower is farther from the leading edge of the leader than at the equilibrium arrangement. This reduces the upwash acting on the leader, leaving a stronger downwash from its own forming vortex. This downwash acts to decrease the effective angle of attack of the leader thereby decreasing its thrust production. This trailing-edge vortex mechanism also applies in a similar way to the case where the follower is perturbed upstream of the equilibrium arrangement.

Figure 5A, 5B, and 5C present flow measurements around the high collective efficiency arrangement where $X^* = 1.7$ and $Y^* = 0$, 0.125, 0.25, respectively, at the dimensionless time of $t^* = 1$. It is observed that the countercloskwise red vortex shed from the leader directly impinges on the follower at $Y^* = 0.125$. Around $t^* = 1$ the time-varying thrust of the follower presented in Figure 5D is seen to maximize at $Y^* = 0.1$ with a pronounced reduction in the thrust for $Y^* > 0.2$. This can be linked to the impinging vortex, which, at this time, induces an upwash on the follower while the follower is pitching through its down-stroke. The upwash then acts to increase the effective angle of attack and thereby increase the thrust production. For the direct impingement location of $Y^* = 0.125$ this effect is maximized, which helps to drive the high efficiency of the collective. However, the

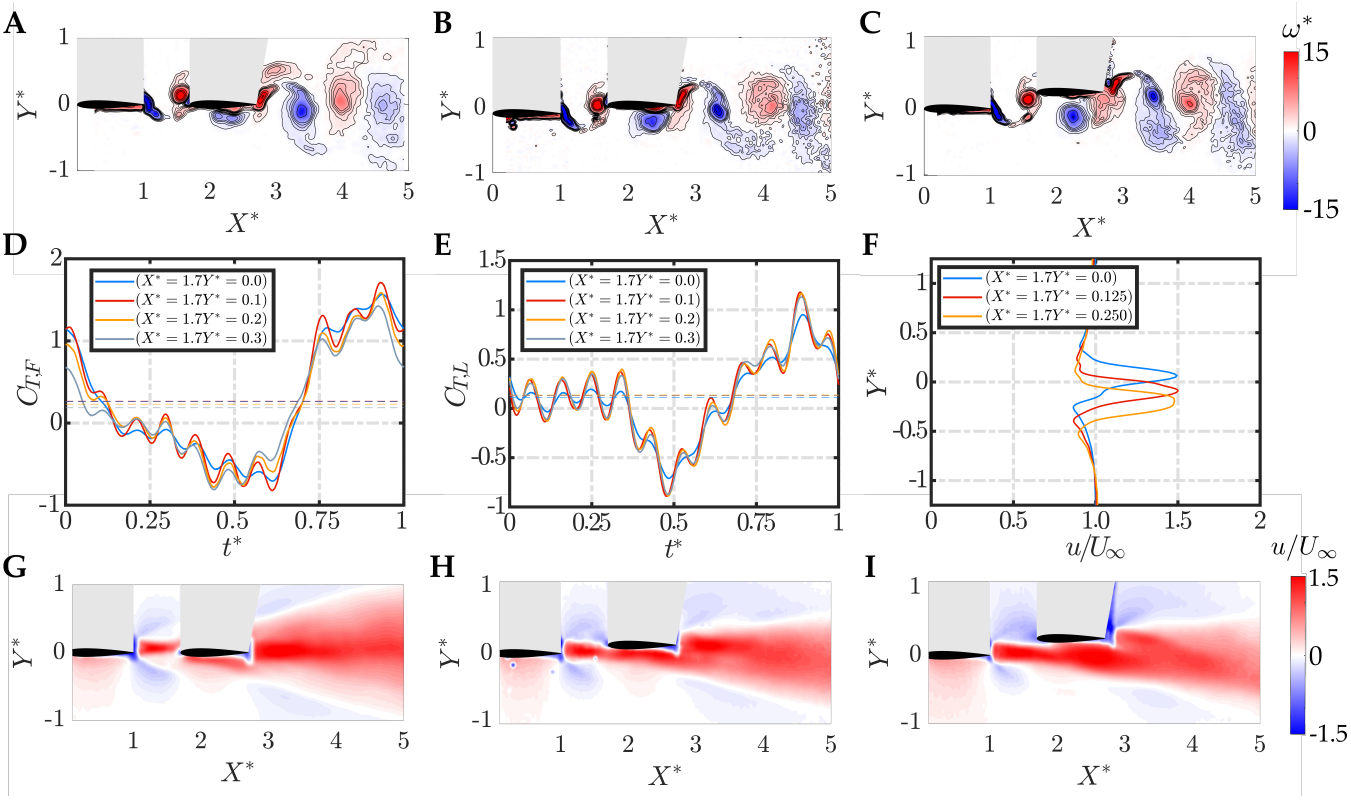

Fig. 5. Vorticity field at $t^* = 1$ during the leader's up-stroke and the follower's down-stroke for (A) the in-line arrangement of $X^* = 1.7$ and $Y^* = 0.0$, (B) the staggered arrangement of $X^* = 1.7$ and $Y^* = 0.125$, and (C) the staggered arrangement of $X^* = 1.7$ and $Y^* = 0.25$. Time-varying thrust coefficient of (D) the leader and (E) the follower, for arrangements of $X^* = 1.7$ and $Y^* = 0.0,\ 0.1,\ 0.2,\ 0.3$. (F) The cycle average x-component of velocity, u/U_∞ at the midpoint between the trailing edge of the leader and the leading edge of the follower at $X^* = 1.35$ for three arrangements of $X^* = 1.7$ and $Y^* = 0.0,\ 0.125$ and 0.25. u/U_∞ presented in (F) is calculated based on the time-averaged flow-fields for the arrangements, (G) $X^* = 1.7$ and $Y^* = 0.0$, (H) $X^* = 1.7$ and $Y^* = 0.125$, and (I) $X^* = 1.7$ and $Y^* = 0.25$.

leader's thrust also plays a role since it slightly increases as the follower moves away from the in-line arrangement to a slightly-staggered arrangement. Figure 5E shows that around $t^* = 1$ the time-varying thrust of the leader is increased slightly when $Y^* \geq 0.1$. This can be understood by examining the mean velocity in the x-direction, u, behind the leader shown in Figure 5G, 5H, and 5I. The momentum jet behind the leader is observed to slightly increase its strength as the follower moves away from the in-line arrangement to a slightly-staggered arrangement. This can be quantified by extracting mean velocity profiles at $X^* = 1.35$, halfway between the leader and follower, and calculating their momentum flux. The extracted profiles are plotted in Figure 5F, and they are used to calculate the momentum flux coefficient as,

$$C_{p_x} \equiv \frac{\overline{p}_x}{1/2\,\rho U_\infty^2 cs} = \int_{Y^*} \left(\frac{u}{U_\infty}\right)^2 dY^*. \qquad [1]$$

The momentum flux coefficients for the $Y^* = 0$, 0.125, and 0.25 cases are $C_{p_x} = 2.74$, 2.75, and 2.76, respectively. This shows a slight increase concurrent with the increase in thrust of the leader as the follower moves from an in-line arrangement to a slightly-staggered arrangement. Taken together the strengthening of the leader's jet and the direct vortex impingement on the follower lead to a maximum in the collective thrust and efficiency for a slightly-staggered arrangement at $X^* = 1.7$ and $Y^* = 0.125$.

Dynamic Schooling Interactions. Within the interaction plane only one *two-dimensionally* stable equilibrium point has been discovered for a side-by-side arrangement. However, this result neglects the effect of dynamic recoil motion of freely swimming bodies, which may alter the physics of these interactions. Dynamic recoil motion occurs when a two-dimensionally unconstrained pitching hydrofoil, for example, pitches through its downstroke. During this stroke a positive lift force is generated leading to a *recoil* motion where the body will heave upward in response to the lift. In this sense, the recoil motion introduces heaving that lags the pitching motion by nearly 180^o, which is known to lower the thrust production (41) and may alter the lift and the stability of an equilibria. In order to explore the effect of these dynamic recoil motions on the stability of the side-by-side equilibrium point, to further verify the findings from the force map, and to determine the *free-swimming* collective performance, freely swimming experiments and simulations were performed.

In the freely swimming experiments the leader foil is still constrained to a fixed position, however, the follower foil is free to move in the X^*-Y^* plane. This is achieved by mounting the follower foil actuation mechanism, for the first time, to a novel double air bearing stage for nearly friction-less motion, and with on-board batteries and wireless communication to eliminate forces from electronic wiring. Exceptional care is taken to align, level, and counter-bend the air-bearing rails in order to minimize these sources of non-hydrodynamic forces acting on the foil. For more details on the unconstrained experimental approach, please see *Unconstrained Foil Experiments*.

To verify that these novel experiments are measuring the actual hydrodynamic forces acting on interacting foils instead of being corrupted by non-hydrodynamic forces, such as settling to a false equilibrium due to rail bending, we have reproduced results of flow-mediated streamwise stable equilibria discovered in (27). Figure 6A presents data from experiments where the follower foil is downstream of the leader in an in-line arrangement. Importantly, the follower is constrained in the cross-stream direction, but unconstrained in the streamwise direction. The graph shows the final dimensionless gap distance of the follower and its final dimensionless streamwise spacing on the vertical left and right axes, respectively, as a function of the synchrony of the follower. The gap distance, $g = X^*c - 1$, is defined in (27) as the distance from the trailing edge of the leader to the leading edge of the follower, and the vortex wake wavelength, λ (measured from particle image velocimetry measurements of an isolated pitching foil), define the dimensionless gap distance or so-called schooling number (25). The initial schooling number defined by the initial distance between the leader and the follower is denoted from small to large values by markers colored from black to white. Note that for these measurements the entire range of synchrony $(0 - 2\pi)$ was examined.

Depending upon the initial schooling number and the synchrony, the follower settles to a streamwise stable equilibria in $\mathcal{O}(10)$ cycles. The final schooling number follows a linear relationship with the synchrony, and for a specific synchrony such as $\phi = \pi$, there are multiple final locations for the follower depending upon its initial schooling number. In fact, the final schooling numbers for $\phi = \pi$ within the data range are $S = 1.5$ and 2.5, which are precisely the same schooling numbers found in (27) for out-of-phase heaving foils. These results validate the capability of the experiments to measure flow-mediated equilibria instead of experimental artifacts.

In a second experiment the follower starts at a range of in-line arrangements, but it is unconstrained in both the streamwise and cross-stream directions. This experiment examines the *two-dimensional* stability of in-line arrangements, which are predicted by the force map data to be unstable saddle points. Figure 6B presents the time-varying trajectories in the X^*-Y^* plane of the follower starting from various initial arrangements. Each datum marks the cycle-averaged position and is colored by the dimensionless time. Depending upon the initial starting position, the follower will either move towards or away from the leader indicating that there is a streamwise unstable equilibria between the starting position clusters. However, the follower gets diverted in the cross-stream direction from the $Y^* = 0$ position and does not settle to a two-dimensionally stable equilibria within the domain boundary as predicted by the force map data. This verifies the finding that equilibria in the wake of the leader are indeed two-dimensionally unstable even up to $X^* = 4.5$.

In a third experiment the domain boundary is shifted such that a side-by-side arrangement may be achieved and the follower is unconstrained in both the streamwise and cross-stream directions while the leader remains fully constrained. From the previous force data the follower is expected to generate more thrust when it reaches a side-by-side arrangement and will consequently swim faster than the constrained leader if the channel flow speed remains at the free-swimming speed for an isolated foil of $u^{iso} = 0.0863 \pm 0.002$ m/s. To account for this the free-stream speed of the channel is increased until the follower remains at a constant X^* location without swimming upstream of the leader. Under these conditions, Figure 7 presents the equilibrium position of the follower relative to the leader in the X^*-Y^* plane for a narrow range of synchrony of $170^o \leq \phi \leq 190^o$. As predicted by the force

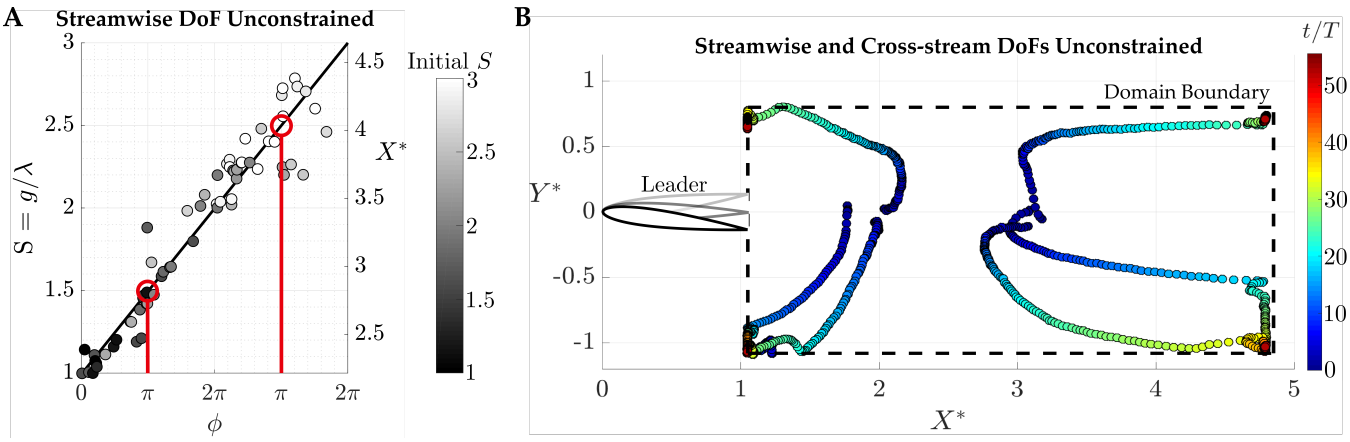

Fig. 6. (A) Equilibrium distance of the in-line arrangement for streamwise unconstrained and cross-stream constrained experiments. The distance S is a function of the synchrony phase ϕ. Marker color is mapped to the initial schooling number. (B) Time-varying trajectories of a fully unconstrained follower (free to move in the X^*-Y^* plane) starting from six different in-line arrangements. The markers represent the position of the follower's leading edge and their color is mapped to the dimensionless time t/T. Dashed lines represent the domain boundaries.

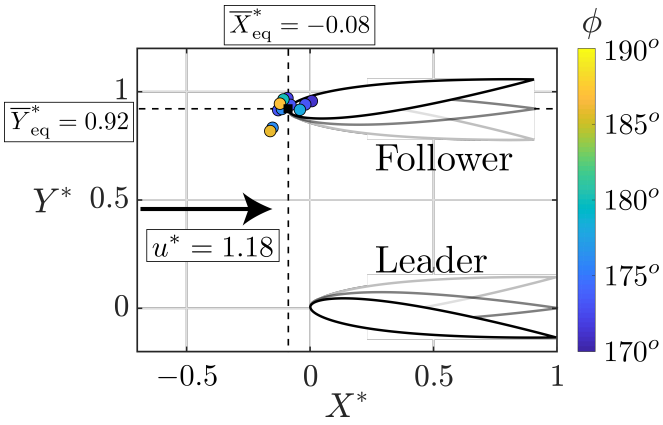

Fig. 7. Equilibrium position of the side-by-side arrangement for a fully unconstrained follower free to move in the X^*-Y^* plane. The equilibrium position markers represent the final positions of individual experiments and their color is mapped to the synchrony of the follower in the range of $170^\circ \leq \phi \leq 190^\circ$. An average equilibrium position is found at $(\overline{X}^*_{eq}, \overline{Y}^*_{eq}) = (-0.08, 0.92)$. The resulting formation achieves a normalized swimming speed of $u^* = 1.18$, which is 18% higher than that of an isolated swimmer.

map for constrained foils, the unconstrained follower settles to an equilibrium position that is nearly a perfect side-by-side arrangement with $\left(\overline{X}^*_{\text{eq}}, \overline{Y}^*_{\text{eq}}\right) = (-0.08, 0.92)$. It is also observed that this stable arrangement is robust to small variations in the synchrony with values below and above $\phi = 180^o$ moving the equilibrium position slightly rearward and forward, respectively. Moreover, for the follower to remain at a streamwise position, the free-stream speed is increased by 18.2% to give a normalized swimming speed of the follower of $u^* = 1.18$. This experiment shows that there is a speed benefit in the side-by-side arrangement and it is indeed stable even when there is dynamic recoil motion.

Finally, to examine whether the side-by-side arrangement remains two-dimensionally stable when both the leader and follower are free to move in the streamwise and cross-stream directions, two freely-swimming hydrofoils are simulated using a potential-flow-based numerical approach. For more details on the numerical approach, please see *Numerical Methods*. Like the constrained experiments, the simulated foils were prescribed sinusoidal pitching motions about their leading edge with an out-of-phase synchrony ($\phi = \pi$). Each foil is assigned with a mass normalized by their characteristic added mass, $m^* = m/(\rho s c^2) = 2.68$, which matches previous work (28) and is comparable to biology (for example, $m^* = 3.86$ was calculated for cod in (42)). Note that the constrained foil measurements presented earlier have an effective dimensionless mass of $m^* = \infty$, since the foils do not exhibit recoil motions. In the simulations, the hydrofoils have a virtual body that is not in the computational domain, but defines parameters applying a drag force to the hydrofoils, following a U^2 high Reynolds number drag law (39).

In free-swimming, the Strouhal number and reduced frequency are *dependent* variables and are outputs of the simulations, while the Lighthill number (see *Numerical Methods*) and dimensionless amplitude are input variables. By fixing the $Li = 0.3$ and varying the dimensionless amplitude over the range $0.3 \leq A^* \leq 0.5$, the Strouhal number is nearly constant at $St \approx 0.3$ since U scales with the amplitude and the pitching frequency as $U \propto fA$ (39, 43, 44) and the reduced frequency varies over the range $0.97 \geq k \geq 0.62$. Table 1 provides further details of the input/output variables for the simulations.

Four cases with varying dimensionless amplitude are considered. Each case was simulated with a range of initial positions for the follower within the region of $-0.2 \leq X^*_0 \leq 0.2$ and $1.0 \leq Y^*_0 \leq 1.6$, with 0.1 chord increments. An example trajectory from case IV is shown in Figure 8A to converge to an equilibrium arrangement after 60 cycles. For each case and all initial positions, the freely-swimming foils are found to converge to an equilibrium point in a side-by-side arrangement as predicted by the constrained and unconstrained foil experiments (see *Supplementary Material* for all of the simulation data). This reveals that a side-by-side arrangement is indeed a two-dimensionally stable arrangement even for freely-swimming foils with dynamic recoil motions.

The simulation data is summarized in Table 1. Note that during self-propelled swimming the dynamic pressure based normalization of the thrust coefficient is equal to the Lighthill number, a fixed quantity in our simulations, so the thrust and power coefficients in the table are normalized by the added

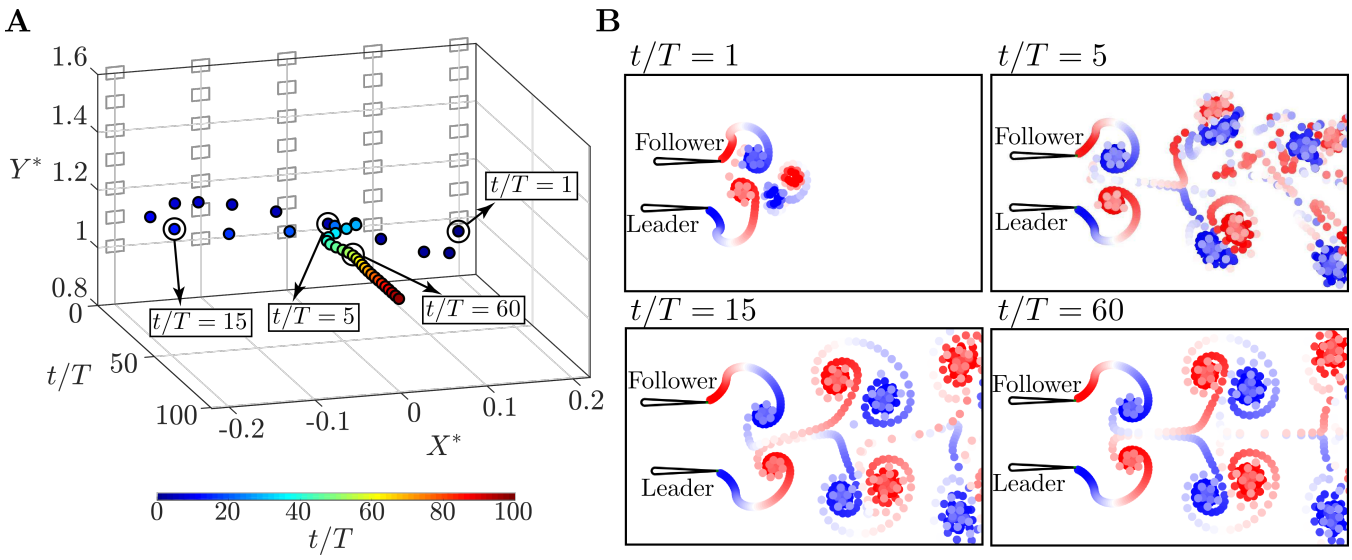

Fig. 8. (A) Trajectory of the follower with respect to the leader leading-edge coordinates over 100 cycles for case IV. The initial positions that were simulated are represented by the gray boxes. The color scale is mapped to the dimensionless time. (B) The leader and follower positions as well as the wake flows are highlighted at dimensionless times of $t/T = 1$, 5, 15, and 60. The period of oscillation is T.

Table 1. Simulation input and output data for four cases of varying amplitude. There are 35 initial positions (X_0^*, Y_0^*) within the region of $-0.2 \leq X_0^* \leq 0.2$ and $1.0 \leq Y_0^* \leq 1.6$ with 0.1 chord increments simulated for each case. This gives a total of 140 simulations. The equilibrium position is denoted as (X_{eq}^*, Y_{eq}^*) and the origin is defined at the leading edge of the leader.

Parameters	Case I	Case II	Case III	Case IV
A^*	0.3	0.35	0.4	0.5
St	0.2914	0.2956	0.2997	0.3076
k	0.9712	0.8445	0.7493	0.6151
(X_{eq}^*, Y_{eq}^*)	(0, 0.7468)	(0, 0.8325)	(0, 0.9239)	(0, 1.0630)
u^*	1.0879	1.0777	1.0691	1.0475
$C_{T,a}^*$	1.1834	1.1624	1.1429	1.0985
$C_{P,a}^*$	1.1120	1.1010	1.0853	1.0660
η^*	1.0641	1.0558	1.0531	1.0306
$C_{T,a}^{iso}$	1.4937	1.4778	1.4622	1.4441
$C_{P,a}^{iso}$	4.5204	4.4757	4.4566	4.660
u^{iso}	0.0899	0.1043	0.1186	0.1473

mass forces instead (see *Numerical Methods*). The data show that in each equilibrium arrangement, the cross-stream foil spacing increases as the reduced frequency decreases. This is the same trend observed previously for a pitching foil in ground effect (28). The swimming speed and the thrust generation are increased by $4-8\%$ and $9-17\%$, respectively, compared to a foil in isolation with more compact arrangements leading to the increased gains. These performance increases originate from increases in the added mass of the foils (see *Collective Performance*) as established recently (33). As in the constrained data, the power and efficiency also increase in a side-by-side arrangement. The power increases by $6-11\%$, and the efficiency increases by $3-5\%$ over a foil in isolation. The thrust and efficiency benefits are observed to be tempered due to the dynamic recoil motions of both foils.

Discussion and Conclusions

For the first time, we have discovered that a side-by-side arrangement of pitching foils is not only *two-dimensionally* stable, but also two-dimensionally *super-stable* where the relative distances between swimmers is constant *and* the school as a whole does not have forces acting on it to drift to one side or the other during locomotion. Indeed, the school is shown to be super-stable for freely-swimming foils, which also enjoy modest speed and efficiency gains over swimming in isolation. This provides new evidence that the Lighthill conjecture (23) may play a role in school formation and spatial patterns of swimmers even if only in a statistical sense akin to birds in a V-formation (10). Indeed, it has been observed (11) that above a critical swimming speed, tetra fish organize in a side-by-side lineup (or phalanx formation as described in the study) and that they enjoy some energetic benefit. Our findings support this previous work and provide a new viewpoint that perhaps the self-organization of the tetra fish is passive in nature and not an active control strategy by the fish.

While this is a provocative result, there are many differences between schooling pitching foils and schooling tetra fish that make it difficult to draw a direct conclusion about the fish. One important difference is that the fish are composed of a body and fins, with it's caudal fin undergoing a combined heaving and pitching motion. However, recent work has shown that both purely heaving and purely pitching foils experience one-dimensional stability in an in-line arrangement (15), so perhaps the difference in kinematics is not consequential for the existence of stable equilibria. Still, further work should aim to examine the passive stability of truly fish-like swimmers to directly answer this question.

Another complicating factor is that it has been argued that three-dimensional swimmers in an infinite school experience breakdown of their shed wake vortices (45), thereby disrupting the coherent vortex-body interactions that drive the in-line and staggered arrangement interactions. The side-by-side interactions, though, are dominated by oscillating dipole flow

fields produced from motions of the nearby bodies, which cannot break down like wake vortices. This may mean that a stable side-by-side arrangement and its performance benefits would hold even for three-dimensional swimmers and/or dense schools. Further work in this direction is also warranted to provide some understanding of how the two-body two-dimensional interactions of the current study translate to many-bodied and three-dimensional interactions.

Previous work (24, 25, 27) has shown that in-line arrangements have multiple *one-dimensionally* stable equilibria, while the current results show that those equilibria, at least in the near-wake of the leader, are in fact unstable in the cross-stream direction. However, this does not indicate that these one-dimensionally stable points are irrelevant, but instead this work highlights that the degree of stability falls along a spectrum. For instance, a fish swimming in the wake of another fish may only need to actively control its cross-stream position in order to maintain a schooling arrangement, which requires less control effort than actively controlling two degrees of freedom, but more effort than controlling none. While higher degrees of stability can relieve needs for control strategies for swimmers and lead to completely passive self-organization, lesser degrees of stability may more subtly sculpt the schooling patterns observed in fish by influencing the trajectory manifolds or the statistical positioning of swimmers. Beyond the translational stability of arrangements, it is unclear whether the orientation of a swimmer will also be stable to perturbations since it is unstable at least for some synchronizations and arrangements (46).

Interestingly, when the thrust and efficiency performance are considered, the ideal arrangement for maximizing performance is not the super-stable side-by-side arrangement, though modest thrust and efficiency benefits can be reaped in this arrangement. The optimal thrust and efficiency performance occurs for a slightly staggered arrangement, which gives rise to interesting questions about whether animals swim in energetically optimal arrangements through more attentive control or in more stable arrangements with less performance benefits.

This study provides a rich understanding of the interplay of stability and performance in schooling pitching foils and these findings reveal hypotheses for understanding biological schooling. These findings also provide insights that aid in the design of multi-finned or schools of bio-inspired machines.

Materials and Methods

Constrained Foil Experiments. Experiments were conducted for a minimal collective consisting of a pair of hydrofoils constrained in space and immersed in a closed-loop water channel, oscillating under prescribed sinusoidal pitching motions about an axis located 8.4 mm behind their leading edge. A constant flow speed of $U = 0.093$ m/s was imposed, which gives a chord-length based Reynolds number of $Re = 9{,}950$. The flow over the hydrofoils was restricted to be nominally two-dimensional by the placement of a surface and splitter plate near the hydrofoil tips. Two identical hydrofoils with a rectangular planform, and NACA 0012 cross-section were designated as the leader and follower. Each hydrofoil had a chord length of $c = 0.095$ m, and a span length of $s = 0.19$ m, which gives an aspect ratio of $AR = 2$.
Particle Image Velocimetry measurements of the flow field were performed in the horizontal (X^*-Y^*) plane at the mid-span of the foils. Phase-averaged results were calculated from a total of 100 measurements for each flow-field. A total of 16 distinct phases $(0, \frac{\pi}{8}, \frac{\pi}{4}, ... \frac{15\pi}{8})$ were captured for all schooling arrangements. The camera used was an Imager sCMOS (2560x2560 pixels), and seeding particles of 11 μm hollow metalic coated plastic spheres were illuminated by a 200 mJ/pulse Nd:YAG laser. Multi-pass, cross-correlation processing of the raw images was employed to obtain the resulting vector fields, with a final interrogation window of 48×48 pixels.

Force Measurements. An ATI Nano43 six-axis force sensor was used to measure the thrust, lift and pitching moment acting on each hydrofoil. An optical encoder recorded the angular position information, which was then used to compute the angular velocity, $\dot{\theta}$, for each hydrofoil. The total instantaneous power input was then calculated as $P_T(t) = M_\theta \dot{\theta}$, where M_θ denotes the pitching moment. Here, the inertial power was determined from the same experiments conducted in air, and was subtracted from the total power, $P_T(t)$, to calculate the instantaneous power input to the fluid, $P(t)$. Force measurements were taken for 100 oscillation cycles from the leader and follower, and each experiment was repeated 10 times. The time-averaged values were calculated for each of these trials, and their mean from 10 trials was calculated to determine the time-averaged total thrust, lift, and power. The profile drag was measured for the static foil in an imposed flow over 20 seconds intervals. Net thrust was determined by subtracting the profile drag acting on the hydrofoil(s) from the time-averaged thrust as follows, $\overline{T}_{\text{net}} = \overline{T} - \overline{D}$. The definitions of the net thrust, C_T, lift, C_L, and power, C_P, coefficients and efficiency, η, are given as follows for the individual hydrofoils:

$$C_T = \frac{\overline{T}_{\text{net}}}{\frac{1}{2}\rho U^2 cs}, \quad C_L = \frac{\overline{L}}{\frac{1}{2}\rho U^2 cs}, \quad C_P = \frac{\overline{P}}{\frac{1}{2}\rho U^3 cs}, \quad \eta = \frac{C_T}{C_P}, \qquad [2]$$

where ρ is the fluid density and s is the span-length of the hydrofoils. Here, we also report collective performance parameters, that is, the average performance from the leader and the follower. The collective force and power coefficients as well as the collective efficiency are denoted with a C subscript and they are defined as,

$$C_{T,C} = \frac{\overline{T}_L + \overline{T}_F}{\rho {U_\infty}^2 cs}, \quad C_{L,C} = \frac{\overline{L}_L + \overline{L}_F}{\rho {U_\infty}^2 cs}, \quad C_{P,C} = \frac{\overline{P}_L + \overline{P}_F}{\rho {U_\infty}^3 cs}, \quad \eta_C = \frac{C_{T,C}}{C_{P,C}}. \qquad [3]$$

Note that, here, the performance coefficients were defined with combined propulsor area, that is $2cs$, cancelling the one-half in the denominator. Collective thrust and power coefficients, and efficiency were reported as normalized values with the corresponding isolated hydrofoil performance metric for comparison, and defined as follows,

$$C_T^* = \frac{C_{T,C}}{2C_T^{\text{iso}}}, \quad C_P^* = \frac{C_{P,C}}{2C_P^{\text{iso}}}, \quad \eta^* = \frac{\eta_C}{\eta^{\text{iso}}}. \qquad [4]$$

Here, the collective performance metrics are compared with the combined values of *two* isolated hydrofoils. The isolated net thrust, drag, power and efficiency are $C_T^{\text{iso}} = 0.10 \pm 0.015$, $C_D^{\text{iso}} = 0.03 \pm 0.002$, $C_P^{\text{iso}} = 0.66 \pm 0.0008$, and $\eta^{\text{iso}} = 0.15 \pm 0.022$, respectively.

Unconstrained Foil Experiments. The unconstrained foil experiments were conducted to simulate a minimal school of two swimmers where the follower is unconstrained (free-to-move) in the X^*-Y^* plane while interacting with the leader. Similar to the constrained foil experiments, two identical hydrofoils with a rectangular planform, NACA0012 cross-section, and aspect ratio $AR = 3$ were designated as the leader and follower. The leader hydrofoil was constrained in both the streamwise (X^*) and cross-stream (Y^*) directions.

Similar to the constrained foil experiments, the foils were prescribed with sinusoidal pitching motions by using a servo motor. The follower receives start/stop commands from a computer via Infrared signal. Each servo motor is controlled by an Arduino MEGA2560. A detailed description of the equipment and data processing can be found in the Supplementary Material.

Numerical Methods. To model the flow over a foil unconstrained both in the streamwise and the cross-stream direction, we used a two-dimensional boundary element method (BEM) based on potential flow theory in which the flow is assumed to be irrotational, incompressible and inviscid. Previously, this method was used to model flow over unsteady hydrofoils (39, 47, 48), and their interaction with a solid boundary and the associated performance for constrained and unconstrained foils (17, 28). Further details about the numerical method used here can be found in previous work (28, 39).

Since the hydrofoils are self-propelled a drag force is applied to them, which follows a high Reynolds number U^2 drag law (49). The drag force is determined by the properties of a virtual body, not present in the computational domain, which are determined by the Lighthill number, Li. This dimensionless number is equal to $Li = C_D S_{wp}$, where C_D is the drag coefficient of virtual body and S_{wp} is a ratio of the wetted area of the virtual body and propulsor to the planform area of the propulsor. This characterizes how the virtual body drag coefficient and the body-to-propulsor sizing affects the balance of the thrust and drag forces. As previously shown in (39), when Li decreases at a fixed frequency and amplitude of motion, free-swimming speed increases. This leads to a decrease in St and consequently, a decrease in the equilibrium distance as reported in (28). In steady-state free-swimming the Li is equal to the dynamic pressure based thrust coefficient, that is $Li = C_T$. To investigate the stability of the side-by-side equilibrium with recoil motions present, the Lighthill number was then set to $Li = 0.3$. This was the lowest value achievable for the numerical stability of the current BEM formulation without wake impingement on the foil bodies, which is a concern due to decreasing equilibrium distance between the foils if the Li takes lower values.

In self-propelled swimming the dynamic pressure based thrust coefficient simply equals the Lighthill number. This is a fixed quantity in the case of the simulations presented in the current study regardless of whether the swimming speed increases or decreases. This means that the standard definition of the thrust coefficient is meaningless in reflecting the thrust increase that leads to higher swimming speeds when two foils are freely swimming side-by-side. Thus, an added mass based thrust coefficient may be used as well as an added mass based power coefficient for consistency (39). They are defined as,

$$C_{T,a} = \frac{\overline{T}}{\rho f^2 A^2 cs}, \quad C_{P,a} = \frac{\overline{P}}{\rho f^2 A^2 U cs}, \quad \eta = \frac{C_{T,a}}{C_{P,a}}. \qquad [5]$$

The normalized added mass based thrust and power, and the normalized swimming speed are,

$$C^*_{T,a} = \frac{C_{T,a}}{C^{\text{iso}}_{T,a}}, \quad C^*_{P,a} = \frac{C_{P,a}}{C^{\text{iso}}_{P,a}}, \quad u^* = \frac{u}{u^{\text{iso}}}, \qquad [6]$$

respectively.

ACKNOWLEDGMENTS. This work was supported by the National Science Foundation under Program Director Dr. Ronald Joslin in Fluid Dynamics within CBET on NSF award number 1653181 and NSF collaboration award number 1921809. Some of this work was also funded by the Office of Naval Research under Program Director Dr. Robert Brizzolara on MURI grant number N00014-08-1-0642.

1. M George, F Bullo, O Campàs, Connecting individual to collective cell migration. *Sci. Reports* **7**, 1–10 (2017).
2. DL Koch, G Subramanian, Collective hydrodynamics of swimming microorganisms: Living fluids. *Annu. Rev. Fluid Mech.* **43**, 637–659 (2011).
3. P Lissaman, CA Shollenberger, Formation flight of birds. *Science* **168**, 1003–1005 (1970).
4. D Weihs, Hydromechanics of fish schooling. *Nature* **241**, 290–291 (1973).
5. VC Wynne-Edwards, *Animal dispersion: in relation to social behaviour.* (Oliver & Boyd, London, UK), (1962).
6. J Tinbergen, *Social behaviour in animals: with special reference to vertebrates.* (Springer Science & Business Media, Berlin, Germany), (2012).
7. T Pitcher, A Magurran, I Winfield, Fish in larger shoals find food faster. *Behav. Ecol. Sociobiol.* **10**, 149–151 (1982).
8. JP Badgerow, FR Hainsworth, Energy savings through formation flight? a re-examination of the vee formation. *J. Theor. Biol.* **93**, 41–52 (1981).
9. EG Drucker, GV Lauder, Locomotor function of the dorsal fin in teleost fishes: experimental analysis of wake forces in sunfish. *J. Exp. Biol.* **204**, 2943–2958 (2001).
10. SJ Portugal, et al., Upwash exploitation and downwash avoidance by flap phasing in ibis formation flight. *Nature* **505**, 399–402 (2014).
11. I Ashraf, et al., Simple phalanx pattern leads to energy saving in cohesive fish schooling. *Proc. Natl. Acad. Sci.* **114**, 9599–9604 (2017).
12. BM Boschitsch, Pa Dewey, AJ Smits, Propulsive performance of unsteady tandem hydrofoils in an in-line configuration. *Phys. Fluids* **26**, 051901 (2014).
13. L Muscutt, G Weymouth, B Ganapathisubramani, Performance augmentation mechanism of in-line tandem flapping foils. *J. Fluid Mech.* **827**, 484–505 (2017).
14. M Kurt, KW Moored, Flow interactions of two-and three-dimensional networked bio-inspired control elements in an in-line arrangement. *Bioinspiration & biomimetics* **13**, 045002 (2018).
15. S Heydari, E Kanso, School cohesion, speed, and efficiency are modulated by the swimmers flapping motion. *arXiv* **2009:**, 1–16 (2020).
16. PA Dewey, DB Quinn, BM Boschitsch, AJ Smits, Propulsive performance of unsteady tandem hydrofoils in a side-by-side configuration. *Phys. Fluids* **26**, 041903 (2014).
17. DB Quinn, KW Moored, PA Dewey, AJ Smits, Unsteady propulsion near a solid boundary. *J. Fluid Mech.* **742**, 152–170 (2014).
18. M Kurt, KW Moored, Unsteady performance of finite-span pitching propulsors in a side-by-side arrangement in *AIAA Aviation, Fluid Dyanmics Conference.* (2018).
19. S Verma, G Novati, P Koumoutsakos, JA Sethian, Efficient collective swimming by harnessing vortices through deep reinforcement learning. *Proc. Natl. Acad. Sci.* **115**, 5849–5854 (2018).
20. L Dai, G He, X Zhang, X Zhang, Stable formations of self-propelled fish-like swimmers induced by hydrodynamic interactions. *J. The Royal Soc. Interface* **15**, 20180490 (2018).
21. AU Oza, L Ristroph, MJ Shelley, Lattices of hydrodynamically interacting flapping swimmers. *Phys. Rev. X* **9**, 041024 (2019).
22. M Kurt, AE Panah, KW Moored, Flow interactions between low aspect ratio hydrofoils in In-line and staggered arrangements. *Biomimetics* **5**, 13 (2020).
23. SJ Lighthill, *Mathematical biofluiddynamics.* (SIAM), (1975).
24. S Ramananarivo, F Fang, A Oza, J Zhang, L Ristroph, Flow interactions lead to orderly formations of flapping wings in forward flight. *Phys. Rev. Fluids* **1**, 1–9 (2016).
25. AD Becker, H Masoud, JW Newbolt, M Shelley, L Ristroph, Hydrodynamic schooling of flapping swimmers. *Nat. communications* **6**, 1–8 (2015).
26. ZR Peng, H Huang, XY Lu, Collective locomotion of two closely spaced self-propelled flapping plates. *J. Fluid Mech.* **849**, 1068–1095 (2018).
27. JW Newbolt, J Zhang, L Ristroph, Flow interactions between uncoordinated flapping swimmers give rise to group cohesion. *Proc. Natl. Acad. Sci.* **116**, 2419–2424 (2019).
28. M Kurt, et al., Swimming freely near the ground leads to flow-mediated equilibrium altitudes. *J. Fluid Mech.* **875** (2019).
29. PW Webb, Kinematics of plaice, Pleuronectes platessa, and cod, Gadus morhua, swimming near the bottom. *J. Exp. Biol.* **205**, 2125–2134 (2002).
30. M Gazzola, M Argentina, L Mahadevan, Scaling macroscopic aquatic locomotion. *Nat. Phys.* **10**, 758–761 (2014).
31. G Li, D Kolomenskiy, H Liu, B Thiria, R Godoy-Diana, On the energetics and stability of a minimal fish school. *PLoS One* **14**, e0215265 (2019).
32. FJ Huera-Huarte, Propulsive performance of a pair of pitching foils in staggered configurations. *J. Fluids Struct.* **81**, 1–13 (2018).
33. A Mivehchi, Q Zhong, M Kurt, DB Quinn, KW Moored, Scaling laws for the propulsive performance of a purely pitching foil in ground effect. *J. Fluid Mech.* **919**, 1–13 (2021).
34. F Ayancik, FE Fish, KW Moored, Three-dimensional scaling laws of cetacean propulsion characterize the hydrodynamic interplay of flukes' shape and kinematics. *J. Royal Soc. Interface* **17** (2020).
35. Y Bao, et al., Dynamic interference of two anti-phase flapping foils in side-by-side arrangement in an incompressible flow. *Phys. Fluids* **29**, 033601 (2017).
36. C Baldwin, Ph.D. thesis (Lehigh University) (2021).
37. N Wagenhoffer, KW Moored, JW Jaworski, Unsteady propulsion and the acoustic signature of undulatory swimmers in and out of ground effect. *Phys. Rev. Fluids* **6**, 1–20 (2021).
38. GJ Dong, XY Lu, Characteristics of flow over traveling wavy foils in a side-by-side arrangement. *Phys. Fluids* **19** (2007).
39. KW Moored, DB Quinn, Inviscid scaling laws of a self-propelled pitching airfoil. *AIAA J.* **57**, 3686–3700 (2019).
40. D Floryan, T Van Buren, CW Rowley, AJ Smits, Scaling the propulsive performance of heaving and pitching foils. *J. Fluid Mech.* **822**, 386–397 (2017).
41. TV Buren, D Floryan, AJ Smits, Scaling and performance of simultaneously heaving and pitching foils. *AIAA J.* **57**, 3666–3677 (2019).
42. E Akoz, KW Moored, Unsteady propulsion by an intermittent swimming gait. *J. Fluid Mech.* **834**, 149–172 (2018).
43. R Bainbridge, The speed of swimming of fish as related to size and to the frequency and amplitude of the tail beat. *J. experimental biology* **35**, 109–133 (1958).
44. M Saadat, et al., On the rules for aquatic locomotion. *Phys. Rev. Fluids* **2**, 083102 (2017).
45. M Daghooghi, I Borazjani, The hydrodynamic advantages of synchronized swimming in a rectangular pattern. *Bioinspiration Biomimetics* **10** (2015).
46. M Gazzola, P Chatelain, WM van Rees, P Koumoutsakos, Simulations of single and multiple swimmers with non-divergence free deforming geometries. *J. Comput. Phys.* **230**, 7093–7114 (2011).
47. J Katz, A Plotkin, *Low-speed aerodynamics.* (Cambridge University Press) Vol. 13, (2001).
48. KW Moored, Unsteady three-dimensional boundary element method for self-propelled bio-inspired locomotion. *Comput. & Fluids* **167**, 324–340 (2018).
49. B Munson, D Young, T Okiishi, *Fundamentals of fluid mechanics.* (Wiley, New York, NY), (1998).